Research Article

Shenghao Jiang*, Macheng Shen, Fatima Rashid Sheykhahmad

Fe_3O_4@urea/HITh-SO_3H as an efficient and reusable catalyst for the solvent-free synthesis of 7-aryl-8*H*-benzo[*h*]indeno-[1,2-*b*]quinoline-8-one and indeno[2′,1′:5,6]pyrido[2,3-*d*] pyrimidine derivatives

https://doi.org/10.1515/chem-2020-0063
received October 21, 2019; accepted March 18, 2020

Abstract: In this study, Fe_3O_4@urea/HITh-SO_3H MNPs as a new, efficient, and recyclable solid acid magnetic nanocatalyst was synthesized and characterized using various methods including Fourier transform infrared spectroscopy, thermogravimetric analysis, scanning electron microscopy, transmission electron microscopy, vibrating sample magnetometry, energy-dispersive X-ray spectroscopy, and X-ray powder diffraction. After the characterization of this new magnetic nanocatalyst, it was efficiently utilized for the promotion of the one-pot synthesis of 7-aryl-8*H*-benzo[*h*]indeno[1,2-*b*]quinoline-8-one and indeno[2′,1′:5,6]pyrido[2,3-*d*]pyrimidine derivatives via three-component reaction of the 1,3-indanedione, aldehyde, and 1-naphthylamine/1,3-dimethyl-6-aminouracil under solvent-free conditions at 80°C. The procedure gave the desired heterocyclic structures in high-to-excellent yields and short reaction times. Also because of the magnetic nature of the nanocatalyst, it can be separated with an external magnetic field and reused at least six runs without any considerable decrease in the catalytic behavior.

Keywords: Fe_3O_4@urea/HITh-SO_3H MNPs, magnetic nanocatalyst, three-component reaction, solvent free

*** Corresponding author: Shenghao Jiang,** School of Engineering and Applied Sciences, Harvard University, 29 Oxford Street, Cambridge, MA 02318, United States of America,
e-mail: ckchangkunck@163.com
Macheng Shen: Department of Mechanical Engineering, Massachusetts Institute of Technology, 77, Massachusetts Ave, Cambridge, MA 02139, United States of America
Fatima Rashid Sheykhahmad: Young Researchers and Elite club, Ardabil Branch, Islamic Azad University, Ardabil, Iran

1 Introduction

The use of magnetic nanoparticles (Fe_3O_4 MNPs) as a core to support the catalyst in organic transformation has become quite popular in chemistry. Because they include unique features such as high dispersion and reactivity, easy separation under external permanent magnetic fields and reusability, pairing with two or multidentate ligands or inorganic structures [1–6]. The use of magnetic nanoparticles may be restricted for reasons such as deformation and aggregation during the chemical process [7]. To remove this restriction and reclaim their features for the specific application, these particles need to be modified by functionalizing their surface via organic or inorganic groups.

Pyrimidine cores are important classes of bioactive and heterocyclic molecules that have received significant importance in the pharmaceutical studies over recent years due to their wide range of therapeutic and pharmacological features such as anticancer [8], anti-inflammatory [9], antimicrobial [10], or antihistaminic activity [11]. Among these compounds, pyrido[2,3-*d*] pyrimidine is one of the main groups of heterocyclic compounds annulated uracil; due to their wide range of medicinal activities such as antibacterial, anticonvulsants, antiaggressive activity, antifolate, antileishmanial, antimicrobial, anti-inflammatory, and inhibitors of cyclin-dependent kinases [12,13]. Thus it is important to prepare the pyrido[2,3-*d*]pyrimidine derivatives. For the one-pot multicomponent preparation, the most common types of compounds are as follow: the reaction of 1,3-indanedione (1 mmol), aryl aldehyde (1 mmol) and 1,3-dimethyl-6-aminouracil (1 mmol) for preparing indeno [2′,1′:5,6]pyrido[2,3-*d*]pyrimidine.

The indenoquinoline derivatives, such as ubiquitous nitrogen-containing heterocycles, play important roles in medicinal chemistry by possessing a diverse spectrum of pharmacological activities such as steroid reductase inhibitors [14], acetylcholinesterase inhibitors [15], antitumor [16,17], and antimalarial activities [18]. Therefore, the synthesis of these heterocyclic compounds is significant for both organic and medicinal chemists. Several applications of quinoline-fused frameworks have already been highlighted in the literature as scaffolds of biological substances, such as ligands for preparing OLED phosphorescent complexes and intermediates in the dyestuffs industry [19–25]. The most common process for synthesizing indeno [1,2-*b*]quinoline diones have been reported via the condensation of 1-naphthylamine (1 mmol), aldehyde (1 mmol), and 2*H*-indene-1,3-dione (1 mmol).

2 Experimental

2.1 General

The chemicals used in this work were obtained from Merck, Fluka, and Aldrich chemical companies and were utilized with any further purification. All melting points were achieved on an Electrothermal 9100 instrument. Fourier transform infrared spectroscopy (FTIR) spectroscopy was done as KBr discs with a Shimadzu spectrometer. Thermogravimetric analysis (TGA) spectra were recorded using a TGA thermoanalyzer (PerkinElmer) instrument. Scanning electron microscopy (SEM) images were obtained using a Tescanvega II XMU Digital Scanning Microscope. Vibrating sample magnetometry (VSM) analyses were performed in a Lakeshore 7407 at ambient temperature. Energy dispersive X-ray spectroscopy (EDX) measurement was performed using ESEM, Philips, and XL30. X-ray powder diffraction (XRD) patterns of samples were obtained using a Siemens D-5000 X-ray diffractometer. Transmission electron microscope (TEM) images were recorded with a TEM Philips EM 208S instrument.

2.1.1 Catalyst synthesis

2.1.1.1 Preparation of the magnetite nanoparticles (Fe_3O_4 MNPs)

About 4.8 g of $FeCl_3{\cdot}6H_2O$ and 1.7 g of $FeCl_2{\cdot}4H_2O$ were dispersed in 100 ml of deionized water by ultrasonication. Then, 10 ml of aqueous ammonia (25%) was added dropwise to the reaction solution under Ar atmosphere by stirring about 30 min with a magnetic stirrer. After the time taken to advance the reaction, the black magnetite precipitate (Fe_3O_4) was rinsed three times with deionized water and dried in vacuum at 60°C.

2.2 Preparation of silica-coated magnetic nanoparticles (Fe_3O_4@SiO_2 MNPs)

One gram of Fe_3O_4 MNPs was added to a mixture including 10 ml deionized water, 45 ml ethanol, and 7 ml of aqueous ammonia solution (25 wt%) and agitated at ambient temperature for about 30 min. After the time required, 6 ml of tetraethylorthosilicate (TEOS) was added dropwise to the reaction vessel and stirred for 24 h under mechanical agitation to afford silica-coated magnetic nanoparticles (Fe_3O_4@SiO_2). Finally, the resulting solid material was isolated using a permanent magnetic field, washed thoroughly with ethanol, and then dried in vacuum at 50°C for 24 h.

2.2.1 Preparation of chloropropyl-functionalized magnetic nanoparticles (Fe_3O_4@CPTES MNPs)

Three grams of the above-synthesized Fe_3O_4@SiO_2 was modified with 6 ml of 3-chloropropyltriethoxysilane (CPTES) in dry toluene (80 ml), and the reaction solution was refluxed under nitrogen atmosphere for 12 h. The obtained Fe_3O_4@CPTES MNPs were filtered with the help of a permanent magnetic field, rinsed thoroughly with dry toluene and diethyl ether, and then dried in vacuum at 80°C for 8 h.

2.2.2 Preparation of urea-functionalized magnetic nanoparticles (Fe_3O_4@CPTES/urea MNPs)

About 2.5 g of Fe_3O_4@CPTES and 10 mmol of urea were added to 50 ml dry toluene and refluxed for 12 h. The resulting black sediment (Fe_3O_4@CPTES/urea MNPs) was filtered with the help of a permanent magnetic field, washed three times with 30 ml of ethanol to remove the unreacted chemicals and dried in vacuum at 50°C for 24 h.

2.2.3 Preparation of Fe_3O_4@urea/HITh MNPs

Two grams of Fe_3O_4@CPTES/urea MNPs was dispersed in 25 ml dry toluene by ultrasonication for half an hour. Subsequently, 0.65 g of 4,5-dihydroxyimidazolidine-2-thione (HITh) and 0.1 ml of trifluoroacetic acid (TFA) were added into the reaction flask, and the mixture was agitated for 1 h at ambient temperature. Then, the resulting solid product was separated by magnetic decantation, washed twice with distilled water (20 ml) and acetone (10 ml) to eliminate the unreacted chemicals, and dried in vacuum at 70°C for 18 h.

2.2.4 Preparation of Fe_3O_4@urea/HITh-SO_3H MNPs

At the end of work, 1 g of Fe_3O_4@urea/HPITh MNPs was dispersed in 25 ml dry dichloromethane by ultrasonication for 30 min and then 10 mmol of 1,4-butane sulfonate was added to the reaction vessel. The reaction mixture was refluxed for 8 h; after this, the resulting solid product was isolated using magnetic decantation. The obtained solid catalyst was rinsed three times with 30 ml of distilled water and dried overnight in vacuum oven at 60°C. This synthesis is exhibited in Scheme 1.

2.2.5 General process for the preparation of 7-aryl-8*H*-benzo[*h*]indeno[1,2-*b*]quinoline-8-one derivatives 4

A mixture containing 1,3-indanedione (1 mmol), aldehyde (1 mmol), 1-naphthylamine (1 mmol), and Fe_3O_4@urea/HITh-SO_3H MNPs magnetic nanocatalyst (10 mg) reacted with each other in a one-pot condensation at 80 °C under solvent-free conditions. To ensure the completion of the reaction, thin layer chromatography (TLC) was used to monitor the reaction mixture. After viewing a single spot on the TLC for the final product, the catalyst was isolated using an external magnet, and the desired pure products were attained from the reaction container by recrystallization from the hot ethanol.

2.2.6 General process for the preparation of indeno[2′,1′:5,6]pyrido[2,3-*d*]pyrimidine derivatives 6

A mixture containing 1,3-indanedione (1 mmol), aldehyde (1 mmol), 1,3-dimethyl-6-aminouracil (1 mmol), and Fe_3O_4@urea/HITh-SO_3H MNPs magnetic nanocatalyst (15 mg) reacted with each other in a one-pot condensation at 80°C under solvent-free conditions. To ensure the completion of the reaction, the reaction mixture was monitored using TLC. After viewing a single spot on the TLC for the desired product, the catalyst was separated by a permanent magnetic field, and the desired pure products were achieved from the reaction container by recrystallization from the hot ethanol.

Ethical approval: The conducted research is not related to human or animal use.

3 Results and discussion

3.1 Catalyst characterization

3.1.1 FTIR analysis of Fe_3O_4@urea/HITh-SO_3H MNPs

Figure 1 exhibits FTIR spectra for Fe_3O_4@CPTES MNPs, Fe_3O_4@urea/HITh MNPs, Fe_3O_4@urea/HITh-SO_3H MNPs,

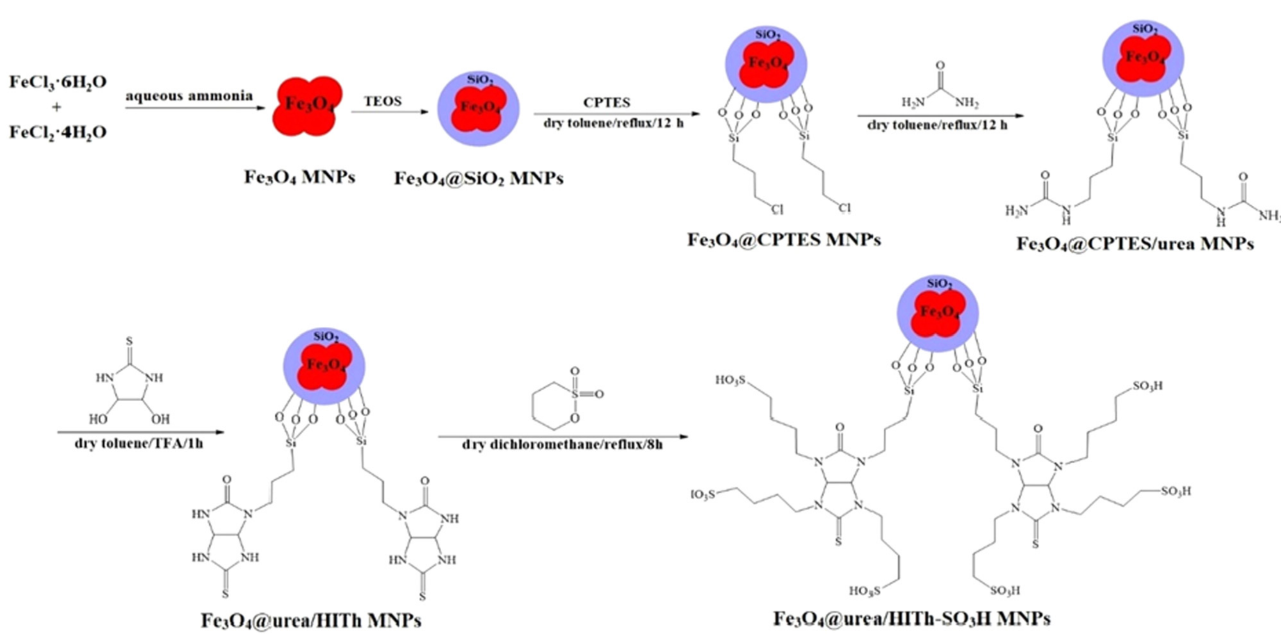

Scheme 1: Synthesis of Fe_3O_4@urea/HITh-SO_3H MNPs.

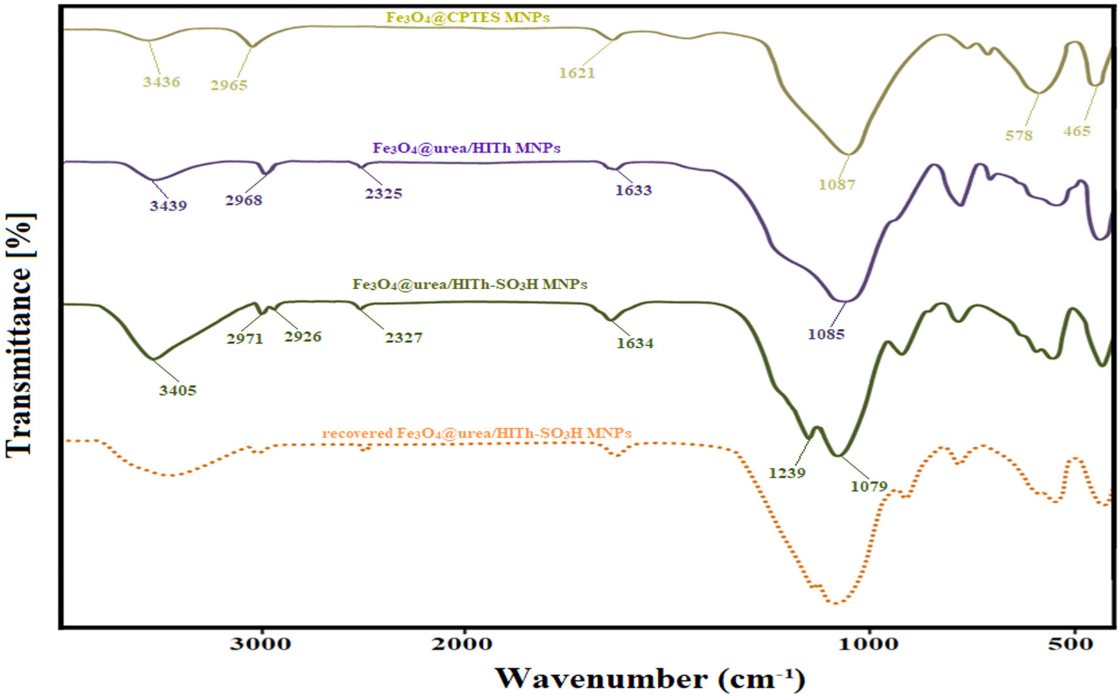

Figure 1: FTIR spectra of Fe_3O_4@CPTES MNPs, Fe_3O_4@urea/HITh MNPs, Fe_3O_4@urea/HITh-SO_3H MNPs, and recovered Fe_3O_4@urea/HITh-SO_3H MNPs.

and recovered Fe_3O_4@urea/HPITh-SO_3H MNPs. The FTIR spectrum for the Fe_3O_4@CPTES MNPs shows a broad peak at 3,436 cm^{-1} that can be attributed to the stretching vibration of the O–H bands, which are linked to the surface of Fe_3O_4 nanoparticles. Two typical absorption peaks at 578 and 465 cm^{-1} can be attributed to the stretching vibration of the Fe–O band of the Fe_3O_4 lattice, while the characteristic peak at 1,087 cm^{-1} corresponds to the Si–O–Si stretching vibration. The existence of a weak peak at 1,621 cm^{-1} comes from vibrations of O–H stretching and twisting bonds of Si–O–H and H–O–H in the silica shell, respectively. The absorption band at 2,968 cm^{-1} is associated with the C–H stretching vibration of 3-chloropropyltriethoxysilane (CPTES) group. The weak absorption peak at 1,633 cm^{-1} is attributable to the C=O stretching vibrations of the amidic group in Fe_3O_4@CPTES/urea MNPs. Moreover, the absorption correlated to C=S peak vibration appears at 2,325 cm^{-1}. The existence of SO_3H groups in the Fe_3O_4@urea/HITh-SO_3H MNPs are claimed with 3,405 and 1,239 cm^{-1} peaks relating to the O–H and O–SO_2 stretching vibration, respectively. It is worth explaining that the FTIR spectra for recovered Fe_3O_4@urea/HITh-SO_3H MNPs after the third recovery and reuse do not show any significant change.

3.1.2 Thermal analysis of Fe_3O_4@urea/HITh-SO_3H MNPs

The TGA corresponding to the Fe_3O_4@CPTES MNPs, Fe_3O_4@urea/HPITh MNPs, and Fe_3O_4@urea/HITh-SO_3H MNPs exhibited information about functional organic groups bonded on the magnetic nanoparticles' surface

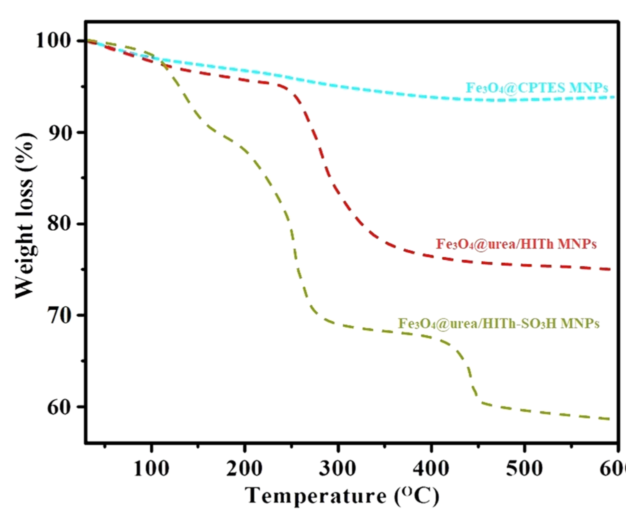

Figure 2: TGA curves of Fe_3O_4@CPTES MNPs, Fe_3O_4@urea/HITh MNPs, and Fe_3O_4@urea/HITh-SO_3H MNPs.

and the thermal stability through the primary loss of mass (Figure 2). TGA data for all cases showed about 4% loss of mass below 150°C because of the loss of the surface O–H groups as well as desorption of a small quantity of adsorbed solvents. From the TGA curve of Fe_3O_4@CPTES MNPs, it can be inferred that the loss of mass was about 7%, which can be chiefly attributed to the CPTES organic functional group on the core–shell structure surface. With further increase in temperature, the TGA curve corresponding to Fe_3O_4@urea/HITh MNPs indicated a more remarkable loss of mass compared with that found in Fe_3O_4@CPTES MNPs. This change in the slope of the curve can be attributed to the decomposition of propyl groups, urea, and HITh on the surface of core–shell structure. Besides the similar loss of mass for all three samples, Fe_3O_4@urea/HITh-SO_3H MNPs have two weight loss steps that are associated with the decomposition of organic functional groups and SO_3H molecules.

3.1.3 SEM analysis of Fe_3O_4@urea/HITh-SO_3H MNPs

Figure 3 shows the morphology and structure of Fe_3O_4@CPTES MNPs and Fe_3O_4@urea/HITh-SO_3H using SEM. Fe_3O_4@CPTES MNPs have a mean particle dimension of about 40 nm (Figure 3a). The SEM micrograph shown in Figure 3b demonstrates clear and vivid changes in the morphology of the Fe_3O_4@urea/HITh-SO_3H, which can be mainly associated with the bonding of acidic groups to the catalyst surface. The particle dimension of Fe_3O_4@urea/HITh-SO_3H MNPs was about 50 nm.

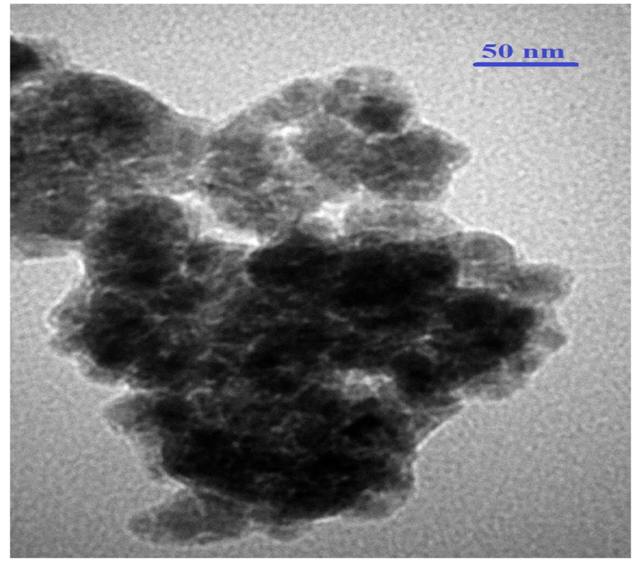

Figure 4: TEM image of Fe_3O_4@urea/HITh-SO_3H MNPs.

3.1.4 TEM analysis of Fe_3O_4@urea/HITh-SO_3H MNPs

TEM image of Fe_3O_4@urea/HITh-SO_3H MNPs is depicted in Figure 4. According to this image, the particle size of the synthesized heterogeneous magnetic nanocatalyst is found to be approximately 17 nm.

3.1.5 VSM analysis of Fe_3O_4@urea/HITh-SO_3H MNPs

To study the magnetic feature of Fe_3O_4 MNPs and Fe_3O_4@urea/HITh-SO_3H MNPs, magnetic measurements were carried out by a room temperature VSM under applied magnetic field (Figure 5). The obtained values

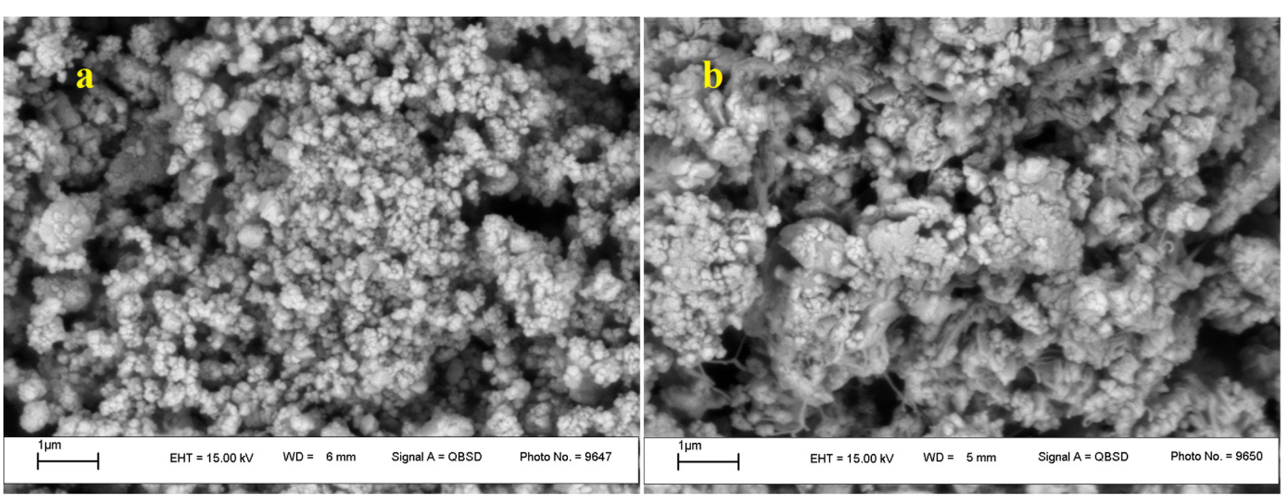

Figure 3: SEM image of (a) Fe_3O_4@CPTES MNPs and (b) Fe_3O_4@urea/HITh-SO_3H MNPs.

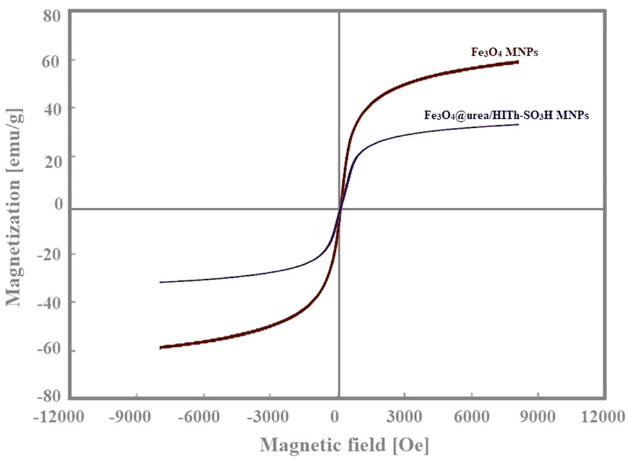

Figure 5: Magnetic curves of Fe$_3$O$_4$ MNPs and Fe$_3$O$_4$@urea/HITh-SO$_3$H MNPs.

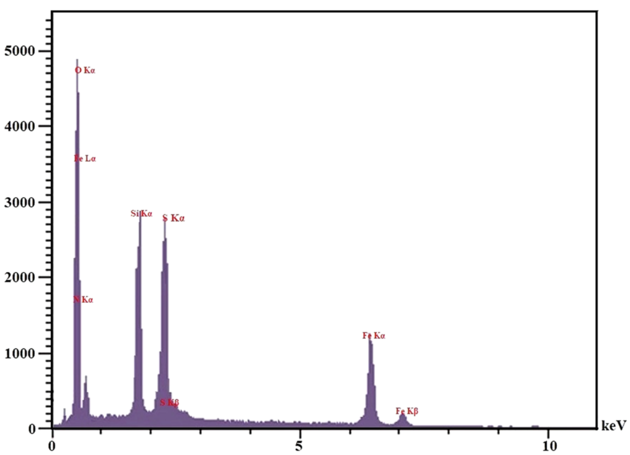

Figure 6: EDX of Fe$_3$O$_4$@urea/HITh-SO$_3$H MNPs.

for the saturation magnetizations of Fe$_3$O$_4$ MNPs and Fe$_3$O$_4$@urea/HITh-SO$_3$H MNPs were 60.29 and 29.35 emu/g, respectively. These values indicate that the magnetic saturation of the catalyst has been reduced. Despite this decline in the magnetic saturation, the heterogeneous magnetic nanocatalyst can still be efficiently isolated from the reaction mixture using a powerful magnet.

3.1.6 EDX analysis of Fe$_3$O$_4$@urea/HITh-SO$_3$H MNPs

The elemental composition of Fe$_3$O$_4$@urea/HITh-SO$_3$H MNPs was obtained using EDX (Figure 6). The EDX spectrum exhibits the characteristic peaks (Fe, O, N, Si, and S) of the catalyst.

3.1.7 XRD analysis of Fe$_3$O$_4$@urea/HITh-SO$_3$H MNPs

The structure of Fe$_3$O$_4$ (a) and Fe$_3$O$_4$@urea/HITh-SO$_3$H MNPs (b) was analyzed using the XRD spectroscopy in the 2θ range of 10°–80°. As shown in Figure 7, XRD of the Fe$_3$O$_4$ MNPs displayed six reflections at 2θ values: 30.08, 35.91, 43.96, 53.78, 57.84, and 63.05, which were marked by the diffractions of (220), (311), (400), (422), (511), and (440), respectively. The same sets of reflections were also obtained for Fe$_3$O$_4$@urea/HITh-SO$_3$H MNPs, indicating the retention of the crystalline structure of Fe$_3$O$_4$ MNPs during surface modification.

This study aimed to publish the rapid and effective preparation of 7-aryl-8*H*-benzo[*h*]indeno[1,2-*b*]quinoline-8-one

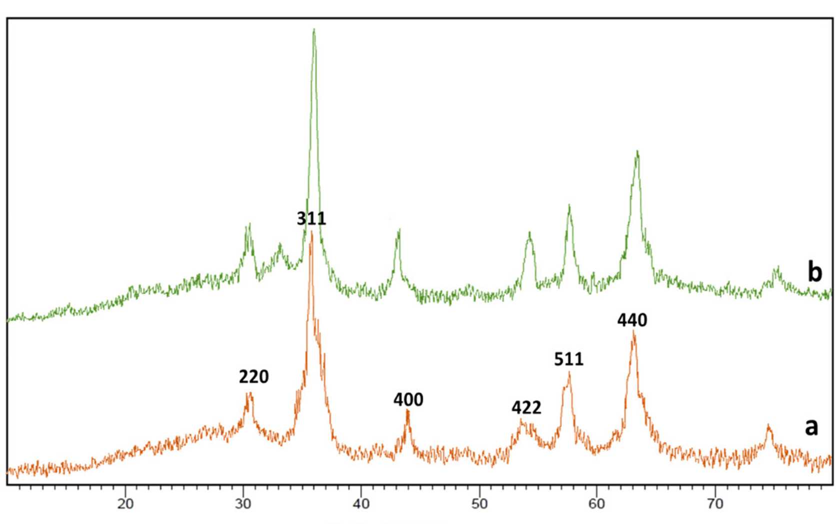

Figure 7: XRD for Fe$_3$O$_4$ MNPs (a) and Fe$_3$O$_4$@urea/HITh-SO$_3$H MNPs (b).

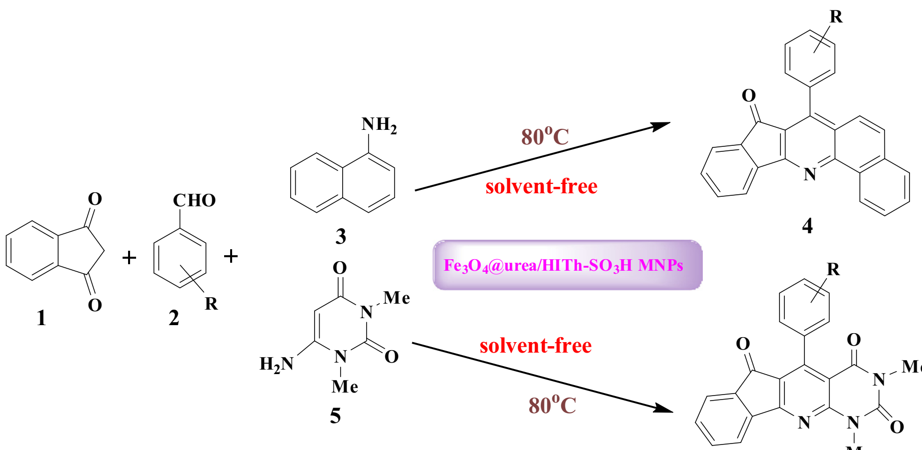

Scheme 2: Production of 7-aryl-8*H*-benzo[*h*]indeno[1,2-*b*]quinoline-8-one **4** and indeno[2′,1′:5,6]pyrido[2,3-*d*]pyrimidine **6** derivatives using Fe_3O_4@urea/HITh-SO_3H MNPs.

and indeno[2′,1′:5,6]pyrido[2,3-*d*]pyrimidine derivatives with lower loading of the new, efficient, and recyclable solid acid magnetic nanocatalyst (e.g., Fe_3O_4@urea/HITh-SO_3H MNPs) under solvent-free conditions (Scheme 2).

To screen the reaction conditions to produce 7-aryl-8*H*-benzo[*h*]indeno[1,2-*b*]quinoline-8-one derivatives, the effect of the solvents, the concentrations of catalyst, and the reaction temperature were explored via the three-component reaction of 1,3-indanedione **1** (1 mmol),

Table 1: Optimizing the three-component reaction of 1,3-indanedione (1), 4-chlorobenzaldehyde (2d), and 1-naphthylamine (3) under different conditions[a]

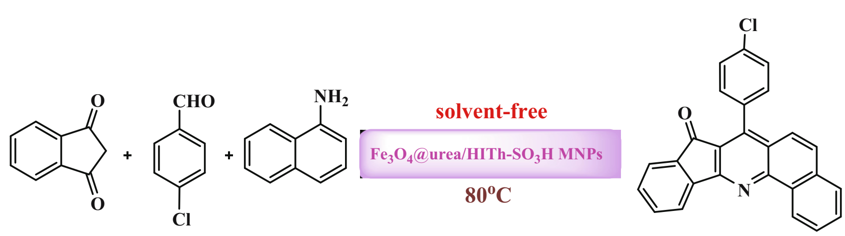

Entry	Solvent	Catalyst (mg)	Temp. (°C)	Time (min)	Yield[b] (%)
1	H_2O	10	Reflux	60	35
2	EtOH	10	Reflux	35	85
3	Solvent free	10	80	4	98
4	Solvent free	—	80	60	Trace
5	Solvent free	15	80	4	95
6	Solvent free	5	80	4	83
7	Solvent free	10	25	60	45
8	Solvent free	10	50	15	78
9	Solvent free	10	60	10	85
10	Solvent free	10	70	8	91
11	Solvent free	10	90	4	96
12	Solvent free	10	100	4	93

[a]Reaction conditions: 1,3-indanedione (1 mmol), 4-chlorobenzaldehyde (1 mmol), 1-naphthylamine (1 mmol), and needed concentration of the catalysts. [b]The yields refer to the isolated product.

Table 2: Fe$_3$O$_4$@urea/HITh-SO$_3$H MNPs-catalyzed synthesis of 7-aryl-8*H*-benzo[*h*]indeno[1,2-*b*]quinoline-8-one derivatives[a]

Entry	RCHO (2)	Product	Yield (%)/time (min)	M.P. (obsd) (°C)	M.P. (°C) [lit.]
1	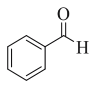	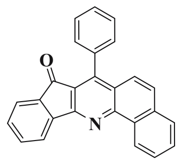 4a	94/6	201–203	202–204 [26]
2	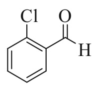	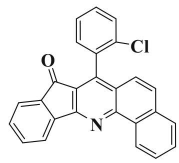 4b	96/4	290–292	289–291 [27]
3	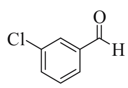	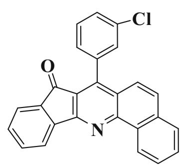 4c	95/5	229–231	230–232 [26]
4	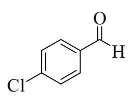	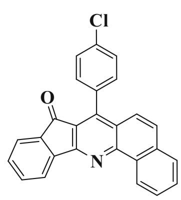 4d	98/4	253–256	259–261 [27]
5	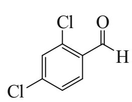	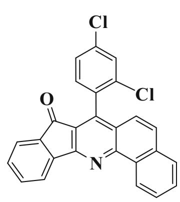 4e	95/7	209–212	212–214 [26]
6	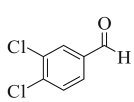	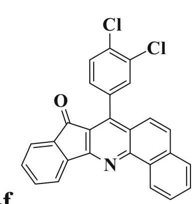 4f	91/8	218–221	220–222 [26]
7	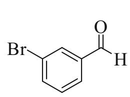	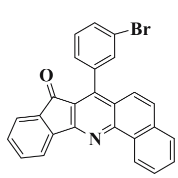 4g	96/6	233–235	236–238 [26]
8	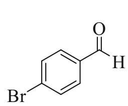	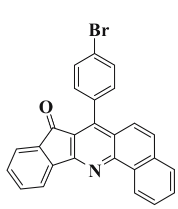 4h	97/5	216–219	218–220 [26]

Table 2: continued

Entry	RCHO (2)	Product	Yield (%)/time (min)	M.P. (obsd) (°C)	M.P. (°C) [lit.]
9	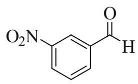	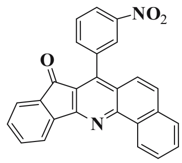 4i	96/6	225–227	222–224 [26]
10	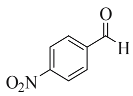	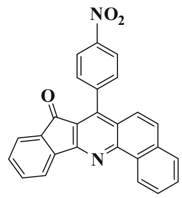 4j	97/5	225–227	210–212 [26]
11	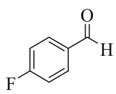	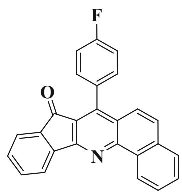 4k	98/6	238–240	231–235 [27]
12	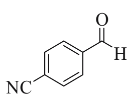	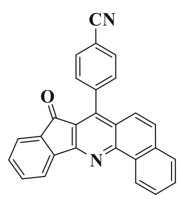 4l	98/8	243–245	240–241 [28]
13	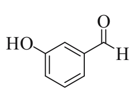	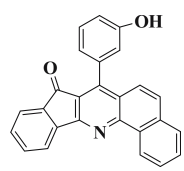 4m	89/12	230–232	228–229 [27]
14	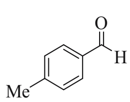	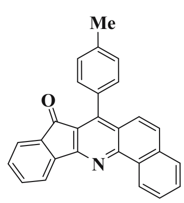 4n	93/10	251–253	256–260 [27]
15	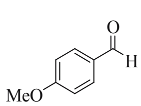	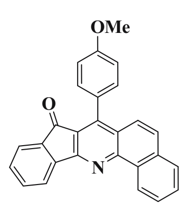 4o	91/10	231–234	233–235 [26]
16	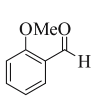	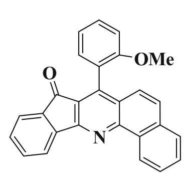 4p	89/12	231–234	233–235 [26]

[a] Reaction conditions: 1,3-indanedione (1 mmol), aldehyde (1 mmol), 1-naphthylamine (1 mmol), and Fe_3O_4@urea/HITh-SO_3H MNPs (10 mg).

Table 3: Optimization of the three-component reaction of 1,3-indanedione (1), 4-nitrobenzaldehyde (2), and 1,3-dimethyl-6-aminouracil (5) under different conditions[a]

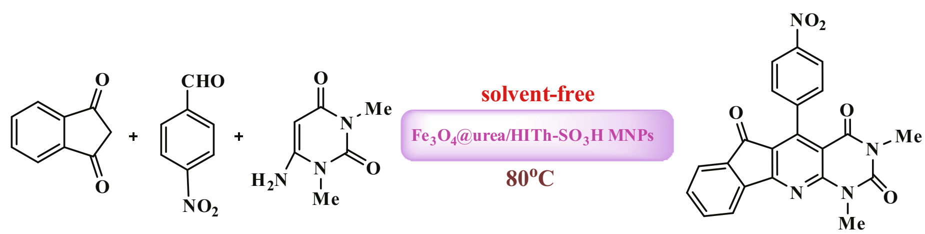

1 2j 5 6j

Entry	Solvent	Catalyst (mg)	Temp. (°C)	Time (min)	Yield[b] (%)
1	H_2O	15	Reflux	60	35
2	EtOH	15	Reflux	35	85
3	Solvent free	15	80	15	96
4	Solvent free	—	80	60	Trace
5	Solvent free	20	80	15	93
6	Solvent free	10	80	15	85
7	Solvent free	15	25	60	42
8	Solvent free	15	50	25	75
9	Solvent free	15	60	20	83
10	Solvent free	15	70	20	90
11	Solvent free	15	90	15	94
12	Solvent free	15	100	15	92

[a]Reaction conditions: 1,3-indanedione (1 mmol), 4-nitrobenzaldehyde (1 mmol), 1,3-dimethyl-6-aminouracil (1 mmol), and needed concentration of the catalysts. [b]The yields refer to the isolated product.

4-chlorobenzaldehyde **2d** (1 mmol), and 1-naphthylamine **3** (1 mmol). The results are listed in Table 1. To attain the optimum reaction solvent, different solvents (e.g., water, ethanol, and solvent-free conditions) were examined in the presence of a certain concentration of catalyst (Table 1, entries 1–3). The reaction gave lower yields when water was utilized as the solvent (Table 1, entry 1). According to the results, the highest reaction yield was obtained when using ethanol as the solvent (Table 1, entry 2). However, the optimal rate and yield were achieved in the absence of solvent for the reaction (Table 1, entry 3). Moreover, the conditions regarding the concentration of catalyst were evaluated on the reaction yield. After numerous screening experiments with different levels of the nanocatalyst, it was observed that using 10 mg of the Fe_3O_4@urea/HITh-SO_3H MNPs was applicable to complete the reaction at the short reaction time (Table 1, entry 3). Enhancing the concentration of catalyst beyond 10–15 mg did not increase the yield (Table 1, entry 5). A low amount of the catalyst required for the reaction from 10 to 5 mg resulted in a decreased yield (Table 1, entry 6). Moreover, when the reaction was conducted in the absence of a catalyst, the product yields decreased remarkably and only a trace level of the desired product was found on TLC, even after the reaction time was prolonged to 60 min (Table 1, entry 4). Also, the effect of temperature was checked on the reaction yield (Table 1, entries 3 and 7–12). It is clear that a low yield of the product was achieved without heating (Table 1, entry 7). The yield of the product was increased at higher temperatures (entries 3 and 8–10). However, a further increase in temperature did not improve the yield of reaction (Table 1, entries 11 and 12).

After optimizing the reaction conditions, the generality of these conditions was studied via multifarious aromatic aldehydes, the outcomes of which are listed in Table 2. It was observed that aromatic aldehydes carrying both different electron-donating and electron-withdrawing groups were subjected to the condensation and in all cases, the relating 7-aryl-8*H*-benzo[*h*]indeno[1,2-*b*]quinoline-8-one derivatives (**4a–p**) were obtained in high-to-excellent yields after the appropriate reaction times.

Table 4: Fe_3O_4@urea/HITh-SO_3H MNPs-catalyzed synthesis of indeno[2′,1′:5,6]pyrido[2,3-*d*]pyrimidine derivatives[a]

Entry	RCHO (2)	Product	Yield (%)/time (min)	M.P. (obsd) (°C)	M.P. (°C) [lit.]
1	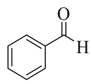	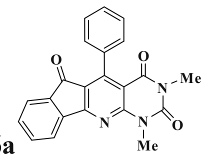 6a	91/15	>300	>300 [34]
2	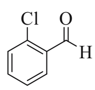	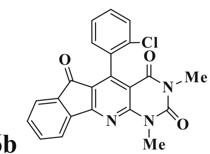 6b	94/15	>300	>300 [33]
3	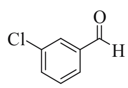	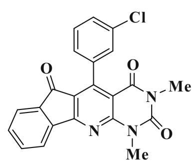 6c	93/18	>300	>300 [35]
4	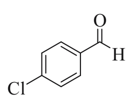	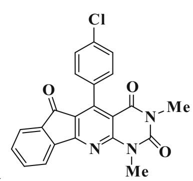 6d	96/15	>300	>300 [32]
5	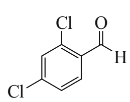	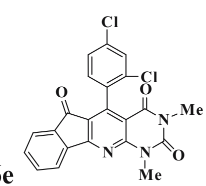 6e	96/18	295–297	297–298 [35]
6	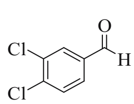	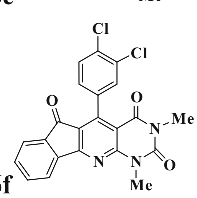 6f	95/20	252–255	253–256 [35]
7	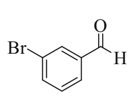	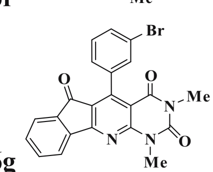 6g	92/15	>300	>300 [33]
8	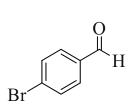	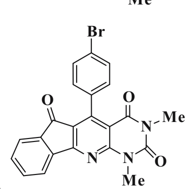 6h	95/12	>300	>300 [35]
9	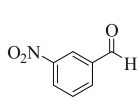	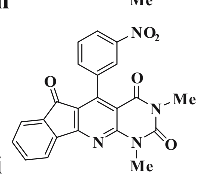 6i	93/15	>300	>300 [32]

Table 4: continued

Entry	RCHO (2)	Product	Yield (%)/time (min)	M.P. (obsd) (°C)	M.P. (°C) [lit.]
10	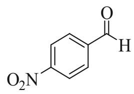	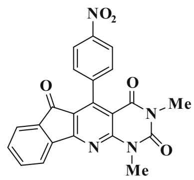 6j	96/15	256–259	258–260 [34]
11	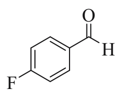	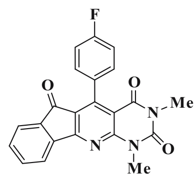 6k	94/12	291–295	294–297 [35]
12	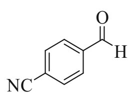	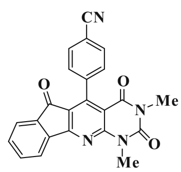 6l	93/10	>300	>300 [33]
13	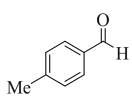	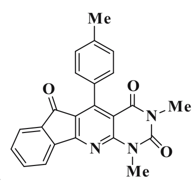 6m	92/20	>300	>300 [33]
14	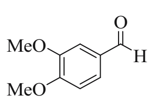	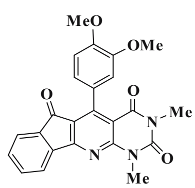 6n	92/22	>300	>300 [35]

[a] Reaction conditions: 1,3-indanedione (1 mmol), aldehyde (1 mmol), 1,3-dimethyl-6-aminouracil (1 mmol), and Fe$_3$O$_4$@urea/HITh-SO$_3$H MNPs (15 mg).

Also, we reported a fast and effective one-pot three-component production of indeno[2′,1′:5,6]pyrido[2,3-*d*] pyrimidine derivatives through the reaction of 1,3-indanedione, aldehyde, 1,3-dimethyl-6-aminouracil in the existence of Fe$_3$O$_4$@urea/HITh-SO$_3$H MNPs (Table 3). To determine the best optimal conditions, we performed the reaction between 1,3-indanedione **1** (1 mmol), 4-nitrobenzaldehyde **2j** (1 mmol), and 1,3-dimethyl-6-aminouracil **5** (1 mmol), in the existence of 15 mg of Fe$_3$O$_4$@urea/HITh-SO$_3$H MNPs at 80°C under solvent-free conditions. The final product **6j** was achieved with an excellent yield (96%) within 15 min (Table 3, entry 3).

Under optimum conditions, the scope and generality of this procedure were explored. To synthesize indeno [2′,1′:5,6]pyrido[2,3-*d*]pyrimidine derivatives, a variety of aromatic aldehydes comprising electron-withdrawing and electron-donating groups in the existence of 15 mg of Fe$_3$O$_4$@urea/HITh-SO$_3$H MNPs were investigated to react with 1,3-indanedione and 1,3-dimethyl-6-aminouracil, and the outcomes are listed in Table 4. It was observed that the above-mentioned aromatic aldehydes produced a high percentage of products in reaction with two other components.

Scheme 3 presents a reasonable pathway for the one-pot three-component condensation of 1,3-indanedione **1**, various aldehyde **2**, 1-naphthylamine **3**/1,3-dimethyl-6-aminouracil **5**, and Fe$_3$O$_4$@urea/HITh-SO$_3$H MNPs. Initially, 1,3-indanedione **1** and carbonyl group of activated aldehyde **2** as the reactant materials react with each other through a Knoevenagel condensation

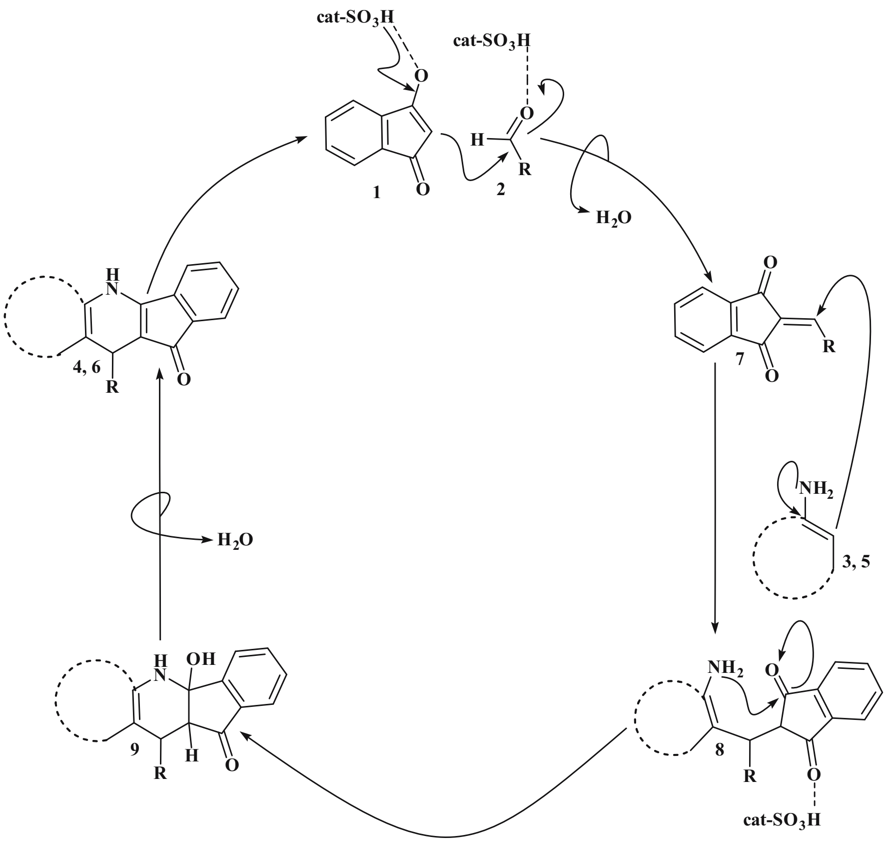

Scheme 3: A probable mechanism corresponding to the one-pot three-component reaction of 1,3-indanedione, aldehyde, and 1-naphthylamine/1,3-dimethyl-6-aminouracil, catalyzed by Fe_3O_4@urea/HITh-SO_3H MNPs under solvent-free conditions.

reaction to obtain intermediate **7**. Then, the polar transition state **8** is obtained by adding 1-naphthylamine **3**/1,3-dimethyl-6-aminouracil **5**, as the C–H-activated acid, via Michael addition to the intermediate **7**. This material is not stable and is converted through cyclization, dehydration, and oxidation to desired products **4**, **6**.

Recyclability is an important merit of any catalysts, therefore, studying the recyclability of the Fe_3O_4@urea/HITh-SO_3H MNPs was necessary (Figure 8). To this end, the reaction was performed using the three-component condensation of 1,3-indanedione (1 mmol), 4-chlorobenzaldehyde (1 mmol), and 1-naphthylamine/1,3-dimethyl-6-aminouracil (1 mmol) in the existence of the catalytic

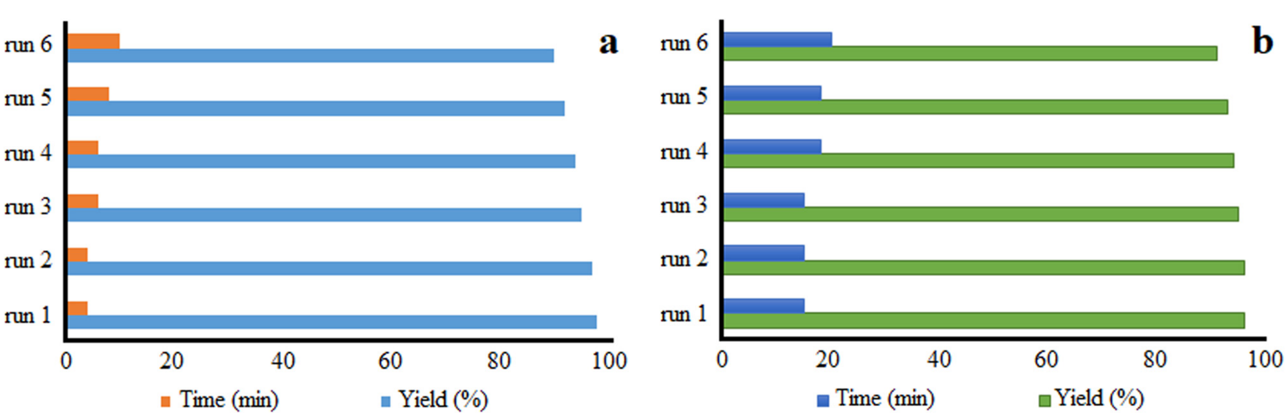

Figure 8: The recycling of Fe_3O_4@urea/HITh-SO_3H MNPs in the preparation of 7-(4-chlorophenyl)-8*H*-benzo[*h*]indeno[1,2-*b*]quinolin-8-one **4d** (a) and 5-(4-chlorophenyl)-1,3-dimethyl-1*H*-indeno[2′,1′:5,6]pyrido[2,3-*d*]pyrimidine-2,4,6(3*H*)-trione **6d** (b) derivatives.

Table 5: Comparison of the outcomes of the production of 7-aryl-8*H*-benzo[*h*]indeno[1,2-*b*]quinoline-8-one and indeno[2′,1′:5,6]pyrido[2,3-*d*]pyrimidine derivatives by means of different catalysts

	Entry	Catalyst and conditions	Reaction time (min)	Yield (%)	Ref.
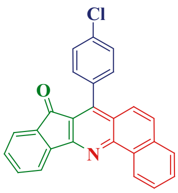	1	Fe_3O_4@cellulose-OSO_3H/solvent-free/40°C	5	40	28
	2	$[Fe(HSO_4)_3]$/DMSO/90°C	210	90	30
	3	P(4-VPH)HSO_4/EtOH/reflux	120	86	29
	4	$H_6P_2W_{18}O_{62}$ $18H_2O$/acetic acid/reflux	360	96	31
	5	TBM/solvent-free/80°C	45	94	26
	7	Fe_3O_4@urea/HITh-SO_3H MNPs/solvent-free/80°C	4	98	This work
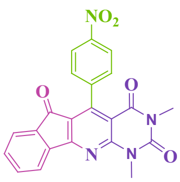	1	$InCl_3/H_2O$/reflux	60	90	32
	2	Co_3O_4-CS-HPA/EtOH/ultrasound	30	92	33
	3	Nano-Fe_3O_4@SiO_2-SO_3H/H_2O/70°C	25	94	34
	4	[bmim]Br/solvent-free/95°C	210	91	35
	5	Nano-Fe_3O_4@cellulose-SO_3H/H_2O/80°C	30	95	36
	7	Fe_3O_4@urea/HITh-SO_3H MNPs/solvent-free/80°C	15	96	This work

level of Fe_3O_4@urea/HITh-SO_3H MNPs at 80°C. At the end of the reaction, the catalyst was isolated from the reaction solution using an external magnet and rinsed with ethanol several times, dried under reduced pressure, and reused in subsequent reactions at least 6 runs without any considerable reduction in the yield of the products.

Efficiency and usability of the catalyst for synthesizing 7-aryl-8*H*-benzo[*h*]indeno[1,2-*b*]quinoline-8-one and indeno[2′,1′:5,6]pyrido[2,3-*d*]pyrimidine derivatives were compared with that of some previously reported catalysts. As presented in Table 5, Fe_3O_4@urea/HITh-SO_3H MNPs is better than previously reported catalysts in saving time, energy, and excellent yields of the products (Table 5).

4 Conclusion

In conclusion, a convenient and effective technique has been designed to synthesize 7-aryl-8*H*-benzo[*h*]indeno[1,2-*b*]quinoline-8-one and indeno[2′,1′:5,6]pyrido[2,3-*d*]pyrimidine derivatives through a one-pot three-component condensation of 1,3-indanedione, aldehyde, and 1-naphthylamine/1,3-dimethyl-6-aminouracil, respectively, using Fe_3O_4@urea/HITh-SO_3H MNPs as a novel heterogeneous magnetic nanocatalyst under solvent-free conditions. Applying an efficient and eco-friendly catalyst, lower loading of the catalyst, magnetical recyclability of the catalyst, omitting organic solvent, simple operation, and high yields of the final products are some benefits of the described protocol. This nanocatalyst was isolated via a permanent magnetic field and recovered efficiently for the six runs without any significant reduction in the catalytic behavior.

Conflict of interest: Authors declare no conflict of interest.

References

[1] Zhang F, Jin J, Zhong X, Li S, Niu J, Li R, et al. Pd immobilized on amine-functionalized magnetite nanoparticles: a novel and highly active catalyst for hydrogenation and Heck reactions. Green Chem. 2011;13:1238–43.

[2] Salavati H, Teimouri A, Kazemi S. Developments of modified magnetic nanoparticle-supported heteropolyacid catalytic performances in dibenzothiophene desulfurization. Iran J Catal. 2017;7:303–15.

[3] Ghasemzadeh MA, Azimi-Nasrabad M, Safaei-Ghomi J. Fe_3O_4@SiO_2 nanoparticles: an efficient, green and magnetically reusable catalyst for the one-pot synthesis of 14-aryl-14*H*-dibenzo[*a*,*i*]xanthene-8,13-dione derivatives. Iran J Catal. 2016;6:203–11.

[4] Zare A, Abi F, Khakyzadeh V, Moosavi-zare AR, Hasaninejad A, Zarei M. Nanomagnetite-Fe_3O_4 as a highly efficient, green and recyclable catalyst for the synthesis of 4,4′-(arylmethylene)-bis(3-methyl-1-phenyl-1*H*-pyrazol-5-ol) s. Iran J Catal. 2015;5:311–20.

[5] Maleki A, Alrezvani Z, Maleki S. Design, preparation and characterization of urea-functionalized Fe_3O_4/SiO_2 magnetic nanocatalyst and application for the one-pot multicomponent synthesis of substituted imidazole derivatives. Catal Commun. 2015;69:29–33.

[6] Rostamnia S, Doustkhah E. Synthesis of water-dispersed magnetic nanoparticles (H_2O-DMNPs) of β-cyclodextrin modified Fe_3O_4 and its catalytic application in Kabachnik–Fields multicomponent reaction. J Magn Magn Mater. 2015;386:111–6.

[7] Hong RY, Feng B, Liu G, Wang S, Li HZ. Preparation and characterization of Fe_3O_4/polystyrene composite particles via inverse emulsion polymerization. J Alloys Compd. 2009;476:612–8.

[8] Ghorab M, Ragab F, Heiba H, Arafa R, El-Hossary RE. In vitro anticancer screening and radiosensitizing evaluation of some new quinolines and pyrimido [4,5-*b*] quinolines bearing a sulfonamide moiety. Eur J Med Chem. 2010;45:3677.
[9] El-Gazzar AR, Hafez H. Synthesis of 4-substituted pyrido-[2,3-*d*]pyrimidin-4(1*H*)-one as analgesic and anti-inflammatory agents. Bioorg Med Chem Lett. 2009;19:3392.
[10] El-Sayed O, Aboul-Enein H. Synthesis and antimicrobial activity of novel pyrazolo[3,4-*b*]quinoline derivatives. Arch Pharm. 2001;334:117.
[11] Quintela J, Peinador C, Botana L, Estévez M, Riguera R. Synthesis and antihistaminic activity of 2-guanadino-3-cyanopyridines and pyrido[2,3-*d*]-pyrimidines. Bioorg Med Chem. 1997;5:1543.
[12] Kanth SR, Reddy GV, Kishore KH, Rao PS, Narsaiah B, Murthy USN. Convenient synthesis of novel 4-substituted-amino-5-trifluoromethyl–2,7-disubstituted pyrido[2,3-d]-pyrimidines and their antibacterial activity. Eur J Med Chem. 2006;41:1011.
[13] Bennett LR, Blankley CJ, Fleming RW, Smith RD, Tessman DK. Antihypertensive activity of 6-arylpyrido [2,3-*d*]pyrimidin-7-amine derivatives. J Med Chem. 1981;24:382.
[14] Brooks JR, Berman C, Hichens M, Primka RL, Reynolds GF, Ramusson GH. Biological activities of a new steroidal inhibitor of δ^4-5α-reductase. Proc Soc Exp Biol Med. 1982;169:67.
[15] Rampa A, Bisi A, Belluti F, Cavalli A, Bartolini M, Cavrini V. SAR of 9-amino-1,2,3,4-tetrahydroacridine-based acetylcholinesterase inhibitors: synthesis, enzyme inhibitory activity, QSAR, and structure-based CoMFA of tacrine analogues. Bioorg Med Chem. 2000;8:497.
[16] Yamato M, Takeuchi Y, Hashigaki K, Ikeda Y, Mingrong C, Takeuchi K, et al. Synthesis and antitumor activity of fused tetracyclic quinoline derivatives. J Med Chem. 1989;32:1295.
[17] Deady LW, Desneves J, Kaye AJ, Finlay GJ, Baguley BC, Denny WA. Synthesis and antitumor activity of some indeno-[1,2-b]quinoline-based bis carboxamides. Bioorg Med Chem. 2000;8:977.
[18] Venugopalan B, Bapat CP, Desouza EP, Desouza NJ. Synthesis of 2- and 3-(4-chlorophenyl-4-hydroxy-7-(4-trifluoromethyl-phenyl)-5,6,7,8-tetrahydro-quinolin-5-one and 5,10-dihydro-11*H*-8-chloroindeno[1,2-*b*]quinolin-10,11-diones as antimalarials. Indian J Chem Sect B Org Chem Incl Med Chem. 1992;31:38.
[19] Mansake RH, Kulka M. The Skraup synthesis of quinolines. Org React. 1953;7:59.
[20] Povarov LS. αβ-Unsaturated ethers and their analogues in reactions of diene synthesis. Russ Chem Rev. 1967;36:656.
[21] Kouznetsov VV. Recent synthetic developments in a powerful imino Diels-Alder reaction (Povarov reaction): application to the synthesis of N-polyheterocycles and related alkaloids. Tetrahedron. 2009;65:2721.
[22] Fadda AA, Etman HA, Amer FA, Barghout M. Azo disperse dyes for synthetic fibres. 3:2-Styrylquinazolone derivatives. J Chem Technol Biotechnol. 1995;62:170.
[23] Bhatti HS, Seshadri S. Synthesis and fastness properties of styryl and azo disperse dyes derived from 6-nitro substituted 3-aryl-2-methyl-4(3*H*)-quinazolinone. Color Technol. 2004;120:151.
[24] Patel VH, Patel MP, Patel RG. Fused heterocycle 11-amino-13*H*-acenaphtho[1,2-e]pyridazino[3,2-*b*] quinazoline-13-one based monoazo disperse dyes. Dyes Pigm. 2002;52:191.
[25] Patel DR, Patel KC. Synthesis, antimicrobial activity and application of some novel quinazolinone based monoazo reactive dyes on various fibres. Dyes Pigm. 2011;90:1.
[26] Mansoor SS, Ghashang M, Aswin K. Facile one-pot synthesis of a novel series of 7-aryl-8*H*-benzo[*h*] indeno[1,2-*b*]quinoline-8-one derivatives catalyzed by tribromomelamine. Res Chem Intermed. 2015;41:6907–26.
[27] Mamaghani M, Hosseyni Larghani T. Ultrasound promoted one-pot three-component synthesis of novel 7-Aryl-8*H*-benzo[*h*]-indeno[1,2-*b*]quinolin-8-Ones under solvent-free conditions. J Chem Res. 2012;36:235–7.
[28] Maleki A, Yeganeh NN. Facile one-pot synthesis of a series of 7-aryl-8*H*-benzo[*h*]indeno[1,2-*b*]quinoline-8-one derivatives catalyzed by cellulose-based magnetic nanocomposite. Appl Organometal Chem. 2017;31:e3814, doi: 10.1002/aoc.3814.
[29] Ghaffari-Khaligh N. Three-component, one-pot synthesis of benzo[*f*]indenoquinoline derivatives catalyzed by poly (4-vinylpyridinium) hydrogen sulfate. Chin J Catal. 2014;35:474–80.
[30] Eshghi H, Nasseri MA, Sandaroos R, Molaei HR, Damavandi S. Ferric hydrogensulfate-catalyzed one-pot synthesis of indeno-[1,2-*b*]quinoline-7-ones. Synth React Inorg Met Org Chem. 2012;42:573–8.
[31] Heravi MM, Hosseini T, Derikvand F, Beheshtiha SYS, Bamoharram FF. $H_6P_2W_{18}O_{62}\cdot 18H_2O$-Catalyzed, three-component, one-pot synthesis of indeno[1,2-b]quinoline-7-one derivatives. Synth Commun. 2010;40:2402–6.
[32] Khurana JM, Chaudhary A, Nand B, Lumb A. Aqua mediated indium (III) chloride catalyzed synthesis of fused pyrimidines and pyrazoles. Tetrahedron Lett. 2012;53:3018–22.
[33] Safari J, Tavakolia M, Ghasemzadeh MA. Ultrasound-promoted an efficient method for the one-pot synthesis of indeno fused pyrido[2,3-*d*]pyrimidines catalyzed by $H_3PW_{12}O_{40}$ functionalized chitosan@Co_3O_4 as a novel and green catalyst. J Organomet Chem. 2019;880:75–82.
[34] Nemati F, Saeedirad R. Nano-Fe_3O_4 encapsulated-silica particles bearing sulfonic acid groups as a magnetically separable catalyst for green and efficient synthesis of functionalized pyrimido[4,5-*b*]quinolines and indeno fused pyrido[2,3-*d*] pyrimidines in water. Chin Chem Lett. 2013;24:370–2.
[35] Shi DQ, Ni SN, Yang F, Shi JW, Dou GL, Li XY, et al. An efficient synthesis of pyrimido[4,5-*b*]quinoline and indeno[2′,1′:5,6]-pyrido[2,3-*d*]pyrimidine derivatives via multicomponent reactions in ionic liquid. J Heterocycl Chem. 2008;45:963–702.
[36] Osanlou F, Nemati F, Sabaqian S. An eco-friendly and magnetized biopolymer cellulose-based heterogeneous acid catalyst for facile synthesis of functionalized pyrimido[4,5-*b*]-quinolines and indeno fused pyrido[2,3-*d*]pyrimidines in water. Res Chem Intermed. 2017;43:2159–74.